Trans Indian Inst Met (2017) 70(8):2205–2211
DOI 10.1007/s12666-017-1044-7

TECHNICAL PAPER

The Influence of Tool Geometry on the Mechanical Behaviour of FSSWed Al/Cu ARBed Composite

M. Shiraly[1] · M. Shamanian[1] · M. R. Toroghinejad[1] · M. Ahmadi Jazani[2] · S. Sadreddini[3]

Received: 15 November 2016 / Accepted: 13 January 2017 / Published online: 25 January 2017

Abstract In the present study, the threaded cylindrical pin and the triangular pin were employed to friction stir spot welding of Al/Cu ARBed composite, and their influence on the material flow and mechanical properties of the spot welds were investigated. Under the same processing condition, higher temperature was measured during friction stir spot welding by using the cylindrical pin, as a result of higher frictional heat and greater material pressed by the pin face, leading to a greater area (volume) and effective length of the stir zone. This, in turn governed by the material flow, resulted in higher shear failure load of the spot welds produced by using cylindrical pin. Nevertheless, asymmetric geometry of the triangular pin appeared to cause higher microhardness around the triangular pin.

Keywords Al/Cu ARBed composite · FSSW · Material flow · Weld strength

1 Introduction

The rising demand for energy saving and environmental issues in different industries, especially automobile and aircraft industries, is a major driving force to reduce weight of components and improve performance [1, 2]. Such interest has created the need to replace steel with Al and/or Mg alloys, as a promising strategy [3]. However, there are very few drawbacks in the use of aluminum. The most notable concerns are the lower mechanical strength and higher cost of aluminum in comparison with iron-based alloys.

Recently, metallic multi-layer composites produced by deformation processes like "severe plastic deformation (SPD)" have been practiced showing high strength and economical merits in order to produce bulk multi-layer composites [4]. Accordingly, Accumulative roll-bonding (ARB) has received a great attention as an innovative and appropriate way of producing aluminum multi-layered composites owing to its lower forming cost and higher productivity rate [5].

The basic goal of the ARB is to prepare ultrafine-grain structures in metals and alloys by means of imposing an extremely high plastic strain on the material, in order to reach a grain structure refinement and strength increase without changing specimen dimensions [6, 7].

In this regard, developing reliable joining techniques, which can enable multi-material design and low cost fabrication processes for high strength aluminum composites, is of great importance. Joining of these materials with conventional fasteners and welding processes such as self-piercing riveting, resistance spot welding and laser spot welding can be markedly difficult and complicated [2, 3]. Therefore, friction stir spot welding (FSSW), as a developed way of the "linear' friction stir welding (FSW), has been applied to generate high-quality joints of sheet metal assemblies [8]. The potential advantages of the spot friction welding process compared to the conventional welding processes are low heat distortion, no need to use protective gases, excellent mechanical properties, very

✉ S. Sadreddini
sina.sadreddini1986@gmail.com

[1] Department of Materials Engineering, Isfahan University of Technology, Isfahan 84156-83111, Iran

[2] Department of Mining and Metallurgical Engineering, Amirkabir University of Technology, Hafez Ave., P.O. Box 15875, Tehran 4413, Iran

[3] Young Researchers and Elites Club, Science and Research Branch, Islamic Azad University, Tehran, Iran

little wastage and pollution and no melting of the base metal, which can then be made readily free of porosity and cracking [9, 10].

The FSSW process, which applies to a lap joint consisting of upper and lower sheets with a backing plate located below the lower sheet to support the external normal loading, can be divided into three steps: (1) tool rotation, (2) tool plunging and stirring, and (3) tool removal. In the second step, frictional heat and deformation, caused by the stirring and the normal force, softens the material. Therefore, the material adjacent to the tool deforms plastically, resulting in the material flow. After retracting the tool, a solid-state bond is created between the upper and lower surfaces of the sheets and a pinhole is left in the weld center [11].

Friction stir spot welds are usually evaluated based on the tensile shear strength of the joint before separation. There are many processing parameters in the FSSW process that affect the joint strength which can be categorized into weld process condition and tool geometry [12].

These individual parameters essentially determine heat generation and material flow around the tool in the spot welds which are closely related to the macrostructure and microstructure evolution of the spot welds as well as weld strength [13].

Badarinarayan et al. [12] reported that the spot welds made with cylindrical-shaped pin showed lower static strength than that with triangular pin, which is ascribed to the difference in the hook geometry. With increasing probe length, the tensile shear strength increases, which is attributed to the effective length of the stir zone [14]. In addition, Lin et al. [11] found that the transient constraint space (TCS), which is constructed with the underside of the shoulder, pin-sheet contact surface and low temperature material region, are the necessary condition for material flow in the friction stir spot welding [11]. However, studies for application of friction stir welding (FSW) technique to Al/Cu Composites have just started and it is imperative to address a thorough understanding of weld condition and weld geometry to investigate the strength of spot welds.

In this work, an investigation has been performed to study the effects of different pin geometries and material flow on the resulting microstructure and weld strength in the friction stir spot welding of Al/Cu ARBed composite.

2 Experimental Methods

500 μm-thick 1050 aluminum foils and 100 μm-thick pure commercial copper foils were employed as raw materials. The dimensions of the individual specimens were 200 mm × 60 mm. Chemical composition of the aluminum alloy is listed in Table 1. Prior to producing the initial sandwich, sheets were degreased in acetone and then scratch brushed to remove surface oxides.

Four aluminum and three copper foils were assembled as a sandwich stack to produce a 2.3 mm thick multilayer sample. Steel wires at four corner points joined the stack tightly to prevent sliding of one over the other. Then, finally, the stack was rolled down at ambient temperature to a 1 mm-thick sandwich. This initial sandwich was cut into two halves and, subsequently, work pieces were degreased, scratch brushed and stacked over each other for further rolling. In this step, concurrent rolling of the stacks of primary sandwich samples with a fixed reduction of 50% in single pass was used, which was repeated up to five times at the room temperature to reduce its thickness from 2.0 to 1.0 mm. Thus, six roll-bonding cycles were performed in total. All experiments were conducted without lubricant on a roll-mill with the roll diameter of 127 mm and speed of 5 rpm. These steps resulted in final multilayered Al/Cu composites of 1-mm thickness using severe plastic deformation. According to the ASTM E8 M standard, the tensile test samples were machined from the ARBed strips, oriented along the rolling direction. The tensile test samples were 6 mm in gage width and 25 mm in gage length. The tensile tests were performed at ambient temperature on a Houndsfield H50KS testing machine at an initial strain rate of 1.67×10^{-4}/s.

20 mm × 70 mm lap-shear specimens were cut from Al/Cu composite sheets and welded in lap configuration on a 40 mm overlapping region. The pre-welding treatment of the specimens was soaking in acetone. The FSSW tool was made from standard tool steel material (H13) with the hardness of 53RC. The tool geometries are shown in Fig. 1.

For the entire test performed in the present research, the tool rotation speed and dwell time were kept constant at 1120 rpm and 4 s, respectively. In this paper, for simplicity of nomenclature, spot welds made using the threaded cylindrical pin and the triangular pin were designated as C1120 and T1120, respectively. To investigate incomplete welds, the threaded cylindrical pins and the triangular pins penetrated to the extent that the shoulder just touched the top surface of the upper sheet.

Welding trials were performed on a conventional milling machine (model FND-32D3). A hole was also drilled approximately at a distance of 10 mm from the pinhole on the top surface of the upper sheet. A K-thermocouple was put into the hole, by virtue of which peak temperatures during the FSSW process were measured. Examinations were performed on the as-welded specimens. We used the normal direction–transverse direction (ND-TD) plane of the sheets at the center of the weld to section the samples. All samples were mechanically polished to prepare them for microstructural observations. The sample microstructures were examined under a scanning electron microscope

Table 1 The chemical composition of aluminum 1050 (wt%)

Si	Cu	Fe	Mn	Mg	Cr	Zn	Ti	Other	Al
0.25	0.05	0.4	0.05	0.05	…	0.07	0.05	0.03	Balance

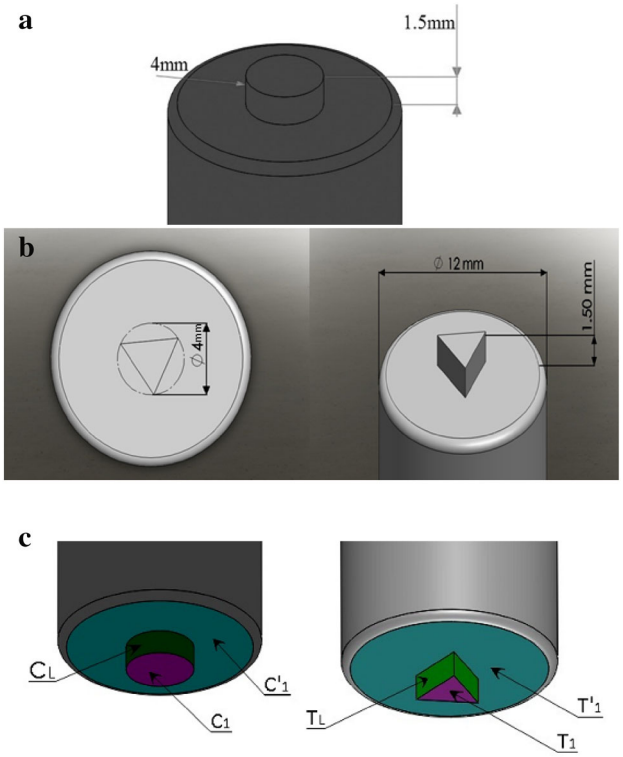

Fig. 1 The tool geometry: **a** cylindrical pin (C1120) and **b** triangular pin (T1120)

(SEM) and a light optical microscopy. The surface area of SZ and length of Cu layers were determined by using Image J software.

Static strengths of the spot welds were evaluated using lap shear testing. The as-welded configuration was used for the lap shear tests. Moreover, to avoid asymmetric force shearing at the welding zone during tensile test, two doublers were attached to the ends of upper and lower sheets. Welded specimens were tested on a tensile machine (Mode Hounsfield H50KS) at a constant crosshead speed of 1.2 mm/min. Each shear failure load reported in the current study corresponded for an average of three measurements. Microhardness tests were performed by Struers Duramin at a load of 10 g and for a period of 10 s on the ND-TD plane. In addition, Microhardness values were averaged randomly at three different points over the 500 μm × 500 μm area. Microhardness was calculated in each case using the following formula

$$HV = 1854 \times L/d^2 \quad (1)$$

where HV is the microhardness in kg/mm^2, L is the load applied in g and d the diagonal of the indention (μm).

3 Results and Discussion

3.1 Microstructure Characterization

The microstructure of welded samples C1120 and T1120 are depicted in Fig. 2. The layered structure of the composite sample (Base Metal) is depicted in the area away from the Weld Zone (denoted as "BM"). Accordingly, the white copper layers in the black aluminium matrix are discernable. Moreover, the stir zone (SZ) and thermomechanically affected zone (TMAZ) in the weld region can be identified. The location of the effective length of stir zone ("d") as obtained by measuring the distance upto the interface of upper and lower sheets, is shown in Fig. 2.

3.2 Temperature

The temperature measurements recorded at a distance of 10 mm from the pinhole are presented in Table 2. As it is evident, temperature in spot welds made with cylindrical pin is found to be slightly higher than that with triangular

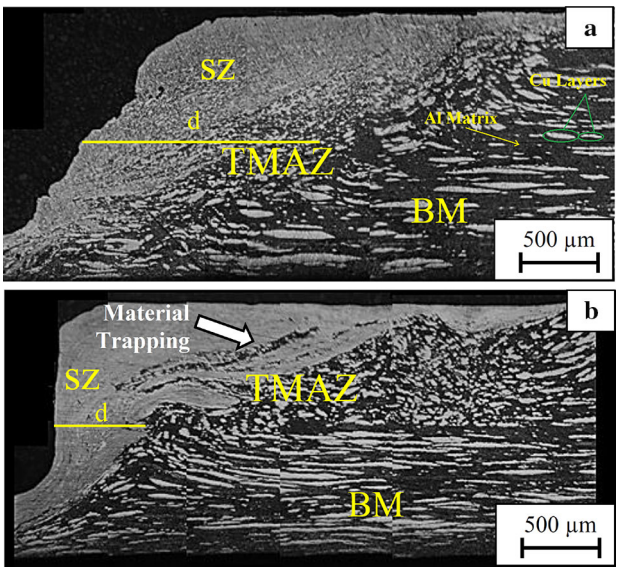

Fig. 2 The microstructure of welded samples showing the different weld geometrical features: **a** C1120, and **b** T1120

Table 2 The measured parameters of FSSW of Al/Cu ARBed composite

Pin geometry	Maximum temperature (°C)	SZ area (mm^2)	Effective length of stir zone "d" (mm)	Shear failure load (N)	Microhardness (HV)
Cylindrical	101	2.1	1.6	1656	239
Triangular	93	1.8	0.6	1475	292

pin, albeit this difference within the keyhole area will be clearly greater, showing higher heat input.

It is to be noted that the designed triangular pin has a circumscribed circle with a diameter equal to the cylindrical pin, leaving similar empty space in the weld region after removal of the welding tool. However, the area involved in the generation of the frictional heat comprises three regions as C_1, C'_1 and C_L for the tool with cylindrical pin and T_1, T'_1 and T_L for the tool with triangular pin (Fig. 1c). As it is evident in Fig. 1c, $C_1 + C'_1$ is equal to $T_1 + T'_1$. It is, therefore, inferred that the difference in the generated frictional heat arises from the lateral surface area (C_L and T_L) of the pins. Accordingly, as T_L (15.52 mm^2) is less than C_L (18.85 mm^2), less frictional heat is expected from the tool with triangular pin when plunged into the work piece. Consequently, higher temperature is attainable by using the cylindrical pin tool.

3.3 Material Flow

In the present work, the variation in length of the copper layers during FSSW of Al/Cu composite is undertaken to investigate the plastic flow of material. In addition, different color of the Cu layers and aluminum matrix makes Cu layers more traceable in the study of material flow. The material flow during the entire FSSW process is divided based on a sequence of two steps: (1) prior to establishing contact with the tool shoulder with the upper sheet, and (2) the complete contact of the shoulder with the upper sheet surface. At the first step, as the tool penetration proceeds, local deformation in the vicinity of the pin periphery is produced [13]. Figures 3 and 4 illustrate the spot welded samples T1120 and C1120 in the absence of shoulder pressure just before touching the upper sheet (step 1).

At this step, the material, softened by the frictional heat, is pushed upward from the lower sheet outside the upper sheet by the pin pressure. The upward material flow demarcates the extruded zone area (EXTD), which is marked by "I" in Figs. 3 and 4. Subsequently, the extruded zone leads to the formation of a triangular region between the EXTD region and the pin. This region marked by II in Figs. 3 and 4 is defined as the Isolated Zone (ISLT). As the plunge depth increases, these regions will gradually develop a well-defined, triangular-shaped stir zone in the spot weld. Fig 2 shows this region after the final stage of

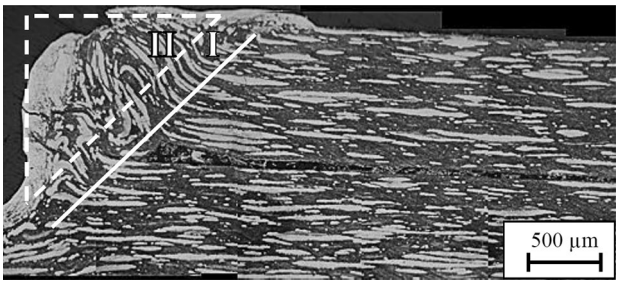

Fig. 3 The microstructural micrograph of the spot samples made with T1120 illustrating the material flow in the absence of shoulder pressure

Fig. 4 The microstructural micrograph of the spot samples made with C1120 illustrating the material flow in the absence of shoulder pressure

development. It is worthy to note that the two legs of the triangle come into direct contact with the welding tool and be influenced by the applied loads from the pin and shoulder.

The Fig. 5 shows the region boundaries of EXTD and ISLT zones made with triangular pin before the shoulder touches the upper sheet at a rotational speed of 1120 rpm. As shown by arrows, in the EXTD zone, the pin pressure forces the sheet material to flow upward, which can be discernable by the upward bending and transferring of the Cu layers. On the other hand, a trend of downward bending and transferring the Cu layers induced by the downward material flow in the ISLT zone is exhibited in Fig. 5.

For C1120, It is obvious that the downward material flow near the pin is caused by the left-handed threads. However, for T1120, it is inferred that a centrifugal material flow inwards toward the sheets by virtue of a rotational motion of material around the pin periphery causes the pressure drop, resulting in the creation of a

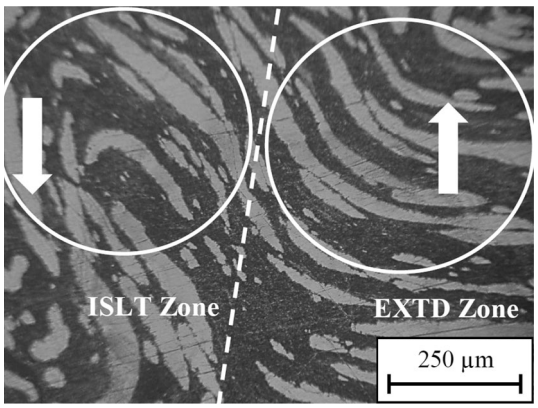

Fig. 5 The region boundaries of EXTD and ISLT zones of T1120 just before the shoulder contacting

cavity. Subsequently, the cavity leads the material to be transferred downward near the rotating pin [13]. As indicated in Fig. 5, a downward flow in ISLT zone is observed. Accordingly, a rotational flow, within the upward and downward coupled motion of materials may be expected. The three aforementioned flows can be depicted in Fig. 6 in a completely welded sample T1120. The upward, downward and the rotational flow of the materials are designated as "a", "b" and "c", respectively.

The second step of the spot welding starts after the shoulder come in close contact with the material to complete the welding (step 2). The crop view of the completely welded sample T1120 is shown in Fig. 7. The Fig. 7 delineates the effect of the shoulder. As the welding tool moves downward to approach the sheet, the tool pin plunges into the upper sheet. Subsequently, prior to establishing the shoulder contact, the upward material flow "a", caused by the effect of downward force and temperature rise, results in extruding a small amount of material from the upper sheet. Following, these materials experience shoulder effect before complete contact occurs.

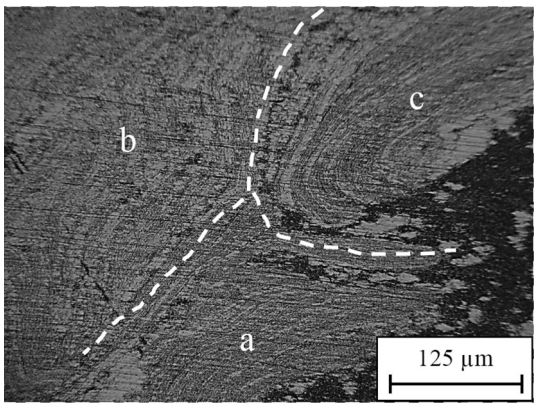

Fig. 6 The three characteristic materials flows in completely welded sample T1120

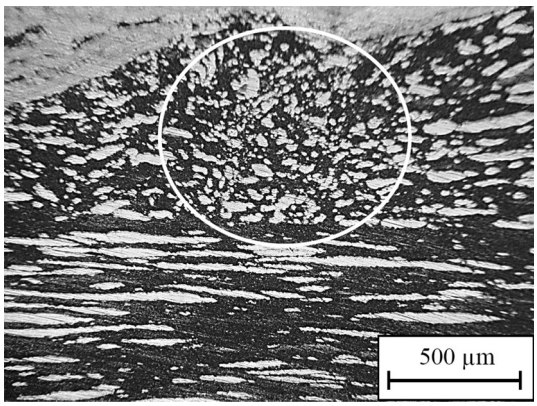

Fig. 7 The crop view of the completely welded sample T1120

Accordingly, as it is evident in Fig. 7, the materials underneath the extruded region in the upper sheet (within the white circle) experience more severe crushing (Cu layer length of 20–50 µm on average) than that in the left side of the white circle (Cu layer length of 100–150 µm on average), which has proximity to the pin.

The observations clearly indicate that the shoulder has a remarkable effect on the material flow by applying a locally downward load to the materials underneath it. To summarize this, the Figs. 8 and 9 of completely spot welded samples T1120 and C1120 are shown. The discussed zones (a, b and c) are evident in the figures. In addition to the mentioned regions, the effect of the shoulder can be demarcated by a region marked as "d". It is worth pointing out that the spot welding using the cylindrical pin has the same regions and mechanisms as the triangular pin for similar reasons.

As it is realized in Figs. 8 and 9, inhibition for evolution of the a, b and c regions into the stir zone (especially in the rotational flow zone "c" and EXTD zone in "a" region) in the spot welds made with triangular pin is more than that with cylindrical pin. It can be explained by the lower heat input generated by using triangular pin (Sect. 3.2). In

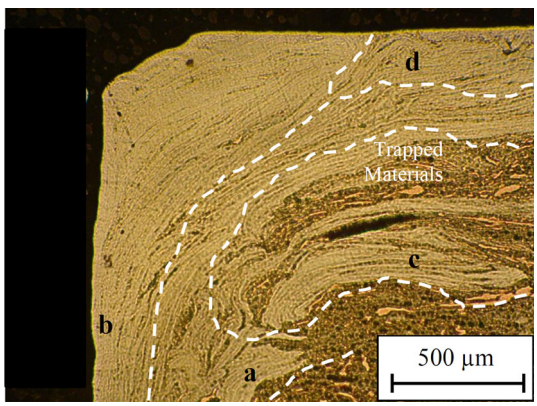

Fig. 8 The completely spot welded sample T1120

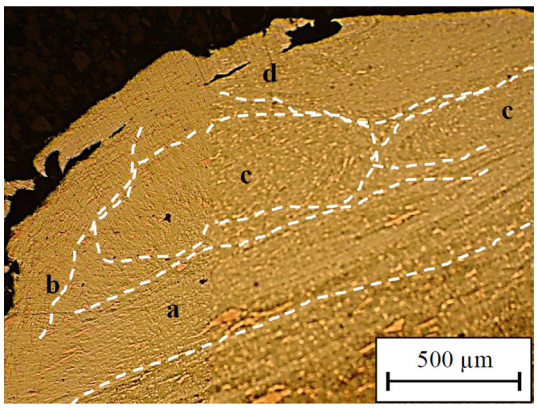

Fig. 9 The completely spot welded sample C1120

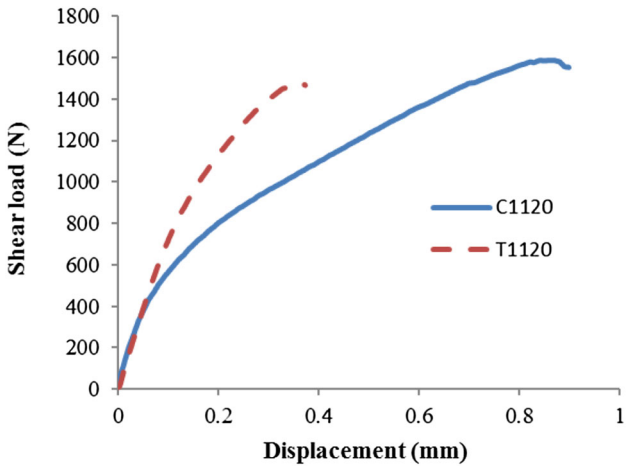

Fig. 10 The typical load–displacement curves for samples C1120 and T1120

addition, the frontal surface area of the pins may be another reason. The frontal surface area of the triangular pin (T_1) (5.19 mm^2) is less than that of cylindrical pin (C_1) (12.56 mm^2), resulting in less material pressured by the pin face when plunging into the workpiece. Consequently, for sample C1120, cylindrical pin can be more effective on evolving the region "a" and rotational flow into the SZ region.

As a result, in spot welds made with triangular pin, a portion of ISLT region, which appears to be trapped as the base metal, is not evolved into the stir zone (Fig. 8). Furthermore, as shown in Figs. 3 and 4, another reason can be inferred from the samples not affected by the shoulder (before step 2). In contrast to the spot welds made with triangular pin (Fig. 3), it is seen in Fig. 4 that a portion of "c" region penetrates into the stir zone (denoted by a black arrow), even before the abolishment of a contact between the shoulder and the upper sheet is established. It is, therefore, clear in the Table 2 that weakness in the formation of three "a", "b" and "c" characteristic regions during welding using triangular pin leads to the shorter effective length of stir zone and smaller area (volume) of the stir zone.

3.4 Weld Strength

The averaged shear failure loads for as-welded specimens are listed in Table 2. The typical load–displacement curves (one of the three samples) for each sample are plotted in Fig. 10. Moreover, the tensile strength of the as-rolled composite is measured to be 224 MPa. It is clear that welded samples made with the cylindrical pin possesses higher shear failure load than that with the triangular pin. Previous studies [9, 15] have reported a direct correlation between shear failure load and the effective length and area of the stir zone. Accordingly, it is inferred that the higher weld strength in the spot welds made with the cylindrical pin can be attributed to the longer effective length of the stir zone and greater stir zone area.

3.5 Microhardness

The average microhardness value of the aluminum matrix of the as-rolled composite is measured to be 68 HV. The objective of this part of the research is to compare the maximum microhardness values between spot welded samples made with the cylindrical and triangular pins. It is indicated (Table 2) that the maximum microhardness measured near the pinhole region for the spot weld made with the triangular pin (292 HV) is higher than that with cylindrical pin (239 HV). The triangular pin possesses an asymmetric geometry with sharp edges. This can result in moving the material back and forth in radial direction around the pin during spot welding. On the other hand, the uniform and symmetric geometry of the cylindrical pin causes the material only to slide around the lateral surface of the pin. It is thus reasonable to expect more material crushing in the vicinity of the triangular pin during welding process. Accordingly, it is conspicuous in the SEM micrographs of the resultant stir zone for samples T1120 and C1120 (Figs. 11, 12) that the stir zone of sample T1120 has finer Cu layers of length (2–5 µm on average) than that of sample C1120 (10–30 µm on average). This consequently results in promoting a higher microhardness.

4 Conclusions

- Friction stir spot welding by means of triangular-shaped and cylindrical-shaped pin was performed on Al/Cu ARBed composite. The potential differences between the spot welds made with the two different

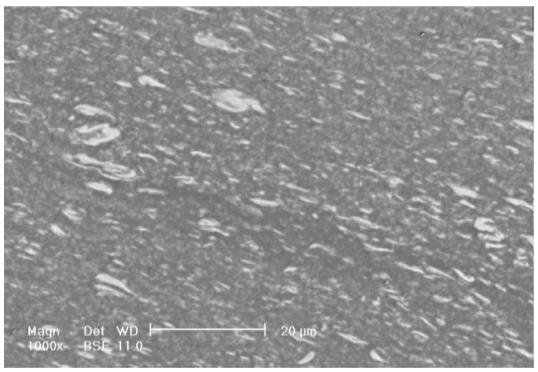

Fig. 11 SEM micrograph of stir zone for sample T1120

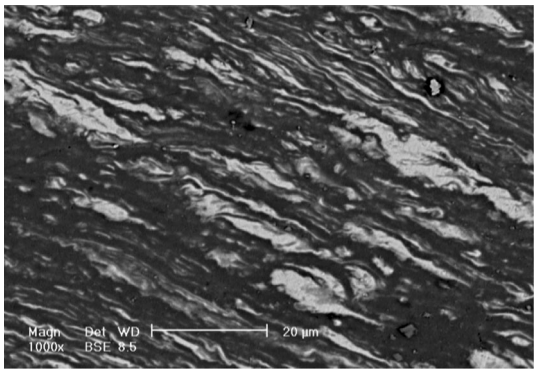

Fig. 12 SEM micrograph of stir zone for sample C1120

pins were discussed. For the cylindrical pin, the experimental observations showed that frictional heat generation was more than that in the spot weld made with the triangular pin.

- The microstructural observations indicated four characteristic regions regarding the material flow for both the triangular and cylindrical pins: (1) The upward motion of the lower sheet material to some distance from the pin (stir zone extremity) due to the pin pressure to its underneath materials, (2) The downward motion of the material near the pin, (3) The rotational motion within the mentioned flows and (4) the effect of the shoulder represented in the upper part of the stir zone.
- For the triangular pin, development of the specified regions within the stir zone (especially the rotational flow and EXTD zone) was more difficult than that of cylindrical pin owing to lower frictional heat and frontal surface area. As a result, area (volume) and effective length of stir zone for sample T1120 was less than sample C1120.
- By virtue of less area (volume) and effective length of stir zone, as a consequence of less pressure applied by the pin face, sample T1120 yielded less weld strength as compared to sample C1120. However, it was indicated that owing to asymmetric geometry of the triangular pin, the hardness of sample T1120, around the pin periphery, was found to be higher when compared to sample C1120.

References

1. [1] Campanelli L C, Suhuddin U F H, Antonialli A Í S, Santos J F D, Alcântara N G D, and Bolfarini C, *J Mater Process Technol* **213** (2013) 515.
2. Mishra R, *Friction Stir Welding and Processing VI*, Wiley, New York (2011).
3. [3] Badarinarayan H, Yang Q, and Zhu S, *Int J Mach Tools Manuf* **49** (2009) 142.
4. [4] Eizadjou M, Talachi A K, Manesh H D, Shahabi H S, and Janghorban K, *J Compos Sci Technol* **68** (2008) 2003.
5. [5] Dehsorkhi R N, Qods F, and Tajally M, *J Mater Sci Eng A* **530** (2011) 63.
6. [6] Toroghinejad M R, Ashrafizadeh F, Jamaati R, Hoseini M, and Szpunar J A, *J Mater Sci Eng A* **556** (2012) 351.
7. [7] Talachi A K, Eizadjou M, Manesh H D, and Janghorban K, *Mater Charact* **62** (2011) 12.
8. [8] Thoppul S D, and Gibson R F, *Mater Charact* **60** (2009) 1342.
9. [9] Shiraly M, Shamanian M, Toroghinejad M R, and Jazani M A, *JMEPEG* **23** (2014) 413.
10. Lohwasser D, and Chen Z (2009) *Friction Stir Welding From Basics to Applications*, Woodhead Publishing Limited, Cambridge.
11. Lin Y C, Liu J J, Chen J N, *JMEPEG* **22** (2013) 3674.
12. [12] Badarinarayan H, Shi Y, Li X, and Okamoto K, *Int J Mach Tools Manuf* **49** (2009) 814.
13. [13] Yang Q, Mironov S, Sato Y S, and Okamoto K, *J Mater Sci Eng A* **527** (2010) 4389.
14. [14] Tozaki Y, Uematsu Y, and Tokaji K, *Int J Mach Tools Manuf* **47** (2007) 2230.
15. [15] Bozzi S, Helbert-Etter AL, Baudin T, Klosek V, Kerbiguet JG, Criqui B, *J Mater Proc Technol* 210 (2010) 1429.